*Journal of the Meteorological Society of Japan*, **99**(2), 269−285, 2021. doi:10.2151/jmsj.2021-013

Special Edition on Global Precipitation Measurement (GPM): 5th Anniversary

# The Synoptically-Influenced Extreme Precipitation Systems over Asian-Australian Monsoon Region observed by TRMM Precipitation Radar

**Hong-Wen JIAN, Wei-Ting CHEN, Peng-Jen CHEN, Chien-Ming WU**

*Department of Atmospheric Sciences, National Taiwan University, Taiwan*

**and**

**Kristen L. RASMUSSEN**

*Department of Atmospheric Sciences, Colorado State University, Colorado, USA*

*(Manuscript received 23 February 2020, in final form 2 November 2020)*

## Abstract

This study investigates the synoptic-scale flows associated with extreme rainfall systems over the Asian–Australian monsoon region (90−160°E and 12°S−27°N). On the basis of the statistics of the 17-year Precipitation Radar observations from Tropical Rainfall Measurement Mission, a total of 916 extreme systems, with both the horizontal size and maximum rainfall intensity exceeding the 99.9th percentiles of the tropical rainfall systems, are identified over this region. The synoptic wind pattern and rainfall distribution surrounding each system are classified into four major types: vortex, coastal, coastal with vortex, and none of above, with each accounting for 44, 29, 7, and 20 %, respectively. The vortex type occurs mainly over the off-equatorial areas in boreal summer. The coast-related types show significant seasonal variations in their occurrence, with high frequency in the Bay of Bengal in boreal summer and on the west side of Borneo and Sumatra in boreal winter. The none-of-the-above type occurs mostly over the open ocean and in boreal winter; these events are mainly associated with the cold surge events. The environment analysis shows that coast-related extremes in the warm season are found within the areas where high total water vapor and low-level vertical wind shear occur frequently. Despite the different synoptic environments, these extremes show a similar internal structure, with broad stratiform and wide convective core (WCC) rain. Furthermore, the maximum rain rate is located mostly over the convective area, near the convective–stratiform boundary in the system. Our results highlight the critical role of the strength and direction of synoptic flows in the generation of extreme rainfall systems near coastal areas. With the enhancement of the low-level vertical wind shear and moisture by the synoptic flow, the coastal convection triggered diurnally has a higher chance to organize into mesoscale convective systems and hence a higher probability to produce extreme rainfall.

**Keywords** extreme rainfall system; Tropical Rainfall Measurement Mission Precipitation Radar; organized convective system; synoptic flows; coastal convection

**Citation** Jian, H.-W., W.-T. Chen, P.-J. Chen, C.-M. Wu, and K. L. Rasmussen, 2021: The synoptically-influenced extreme precipitation systems over Asian-Australian monsoon region observed by TRMM Precipitation Radar. *J. Meteor. Soc. Japan*, **99**, 269–285, doi:10.2151/jmsj.2021-013.

Corresponding author: Wei-Ting Chen, Department of Atmospheric Sciences, National Taiwan University, No.1 Sec. 4 Roosevelt Rd, Taipei 10617, Taiwan
E-mail: weitingc@ntu.edu.tw
J-stage Advance Published Date: 2 December 2020

## 1. Introduction

Extreme rainfall events can induce severe disasters such as landslides and flash flooding and consequently threaten human lives, properties, and infrastructure. However, the representation of precipitation processes, especially extreme rainfall and convection organization, remains a great challenge in current global models, and large-scale circulations and synoptic weather patterns are better simulated. Detailed understanding of convection systems and synoptic flows associated with the extreme rainfall events is imperative not only to the early warning and forecast of these events but also to the appropriate projection of their future occurrence in a changing climate. Over mid-latitudes, synoptic-scale systems are usually directly associated with extreme rainfall events (e.g., Yokoyama et al. 2020; Hamada and Takayabu 2018; Shimpo et al. 2019). However, over the tropical to subtropical areas, heavy rainfall can be directly embedded within synoptic-scale systems such as typhoons and fronts (Su et al. 2012), but they can also involve multiple scales, such as interactions between the MJO and cold surge resulting in intense rainfall near Borneo (Lim et al. 2017). In the case of cross-scale convective interactions, the synoptic-scale influence is usually more difficult to identify.

Previous studies have gained important understanding of the occurrence and internal structure of convective systems accompanied by intense rainfall in the tropics using satellite observations such as the Tropical Rainfall Measurement Mission (TRMM). Hotspots of extreme systems concentrate over coastal areas, such as the Maritime Continent, East coast of Asia and America, and the Bay of Bengal, and they are mostly organized mesoscale systems (Hamada et al. 2014; Zipser et al. 2006; Liu et al. 2008; Liu et al. 2008a; Liu 2011; Houze et al. 2015). The topography, low-level jet, mid-level water vapor, and organized convective structure have been identified as key factors for the generation of extreme rainfall over these coastal areas (Goswami et al. 2010; Rasmussen and Houze 2012; Houze et al. 2011; Sato 2013). Interactions between the large-scale environment, topography, and land–sea breezes near coastlines play a dominant role in triggering coastal convection with extreme rainfall, and the large-scale convergence and abundant water vapor in the synoptic environment provide dynamic and thermodynamic conditions favorable for convective development and organization.

For example, coastal mesoscale convective systems (MCS; Houze 2004) are a major cause of summertime intense rainfall and flooding in southern Taiwan (Jou et al. 2011; Davis and Lee 2012; Xu et al. 2012). The southwesterly flow associated with the summer monsoon brings warm and moist air into the island and leads to an unstable environment. Under the interaction of land–sea breezes, which are a response to diurnal heating, the land breeze in the nighttime creates a convergence zone along or near the coast. As rain falls on the island, the accompanied cold pool forms another barrier to lift the moist southwest prevailing winds. Under these conditions, the resulting convective systems are likely to become MCSs and produce extreme rainfall along the coastal region (Xu et al. 2012). This synoptic southwesterly flow can result from seasonal variations, monsoon trough, or large-scale weather systems like tropical cyclones (TC). Bagtasa (2019) showed that in the northwest Philippines, more than 90 % of high precipitation events coincide with a TC in North West Pacific, even though most of these TCs did not make landfall in the Philippines. The flow from TCs intensifies the water vapor flux in the monsoon trough, and the convergence zone shifts from the South China Sea toward the Philippines. In addition to the synoptic flow pattern, the convective environment accompanied by the synoptic circulation is also critical to the formation of organized convective systems. Tsai and Wu (2017) showed that regions with low-level wind shear ($> 2$ m s$^{-1}$ (100 hPa)$^{-1}$ between 1000 hPa and 850 hPa) and high column water vapor (CWV $> 45$ mm) are associated with large and intense convective systems using a cloud-resolving model. These organized convective systems tend to contain multiple convective cores, and therefore, they have a higher probability to produce heavy rainfall.

This research aims to improve understanding of the linkage between extreme rainfall and its environment based on different synoptic states. A system-based method can provide comprehensive understanding of the relationships between the extremes and their environments. The 17-year observational TRMM dataset provides not only adequate data to be statistically representative but also finer three-dimensional resolution to investigate the differences of the internal structure. Therefore, we will build a system-based dataset from TRMM Precipitation Radar (PR) observations for searching the extreme rainfall events and will classify them based on different synoptic states. Section 2 gives a brief notion of the data used in this study and introduces the method of identifying extreme rainfall systems from the TRMM PR observations. Section 3 depicts the case studies and classification of the synoptic environments associated with the extreme

systems and the spatial and temporal distribution of each category. Discussion and summary are presented in Sections 4 and 5, respectively.

## 2. Method and data

### *2.1 Datasets*

To build up a system-based dataset, we use 17 years of TRMM PR 2A25 version 7 product, near-surface rain rate, from January 1998 to October 2014 in this study. Because the inclination of TRMM's orbit is 35°, the regions near 34°S and 34°N are sampled the most, whereas the equatorial regions are sampled the least (Hirose et al. 2017a). Considering the consistency of the sampling number, the region that we will investigate is between 30°S to 30°N and 180°W to 180°E, which is defined as the tropical region in this study.

This study uses the near-surface rain rate retrieved by the spaceborne Ku-band (13.8 GHz) PR to define rainy systems and to obtain the size and rainfall intensity of each system. The near-surface rain rate is defined as the rain rate at the lowest vertical radar bin and is retrieved from the radar reflectivity. Only the data flagged as "rain certain" in the 2A25 rain flag are chosen. Since microwaves cannot penetrate the deep and dense convective systems, the near-surface rain rate may be underestimated, especially for systems over land (Sato 2013; Kirstetter et al. 2012; Rasmussen et al. 2013). Therefore, we mainly focus on the rainy systems over the ocean and coastal regions. In the case studies (Section 3.1) and the discussion (Section 4), we also examine the vertical structures of the extremes using three-dimensional radar reflectivity and 30-dBZ echo top from PR 2A25.

The Lightning Imaging Sensor (LIS) is a visible band (777.4 nm) image sensor that can detect lightning from the pulse of illumination (emitted from lightning). It estimates the flash counts from the number of illumination pulses in the view time of each footprint. LIS can detect the total flash counts in thunderstorms. Although there is tuning of orbit height, the horizontal resolution of these two sensors is about 5 km in nadir. To assure that every longitude–latitude grid box has enough sampling numbers, all of the orbital data are remapped into 0.1° (about 10 km) horizontal resolution and sorted hour by hour.

To obtain the overall precipitation areas, cloud coverage, synoptic flow, and column moisture of the extreme systems, we also use observation data from TRMM 3B42 and Moderate Resolution Imaging Spectroradiometer (MODIS), as well as reanalysis data from ECMWF interim (Dee et al. 2011). TRMM 3B42 (Huffman et al. 2007) provides 3-hourly rain rate retrievals over 45°S–45°N at a 0.25° latitude–longitude resolution by combining radar, infrared, and microwave signals. MODIS L2 cloud product (Weisz et al. 2007) provides the cloud top temperature (CTT) at the infrared channel (11 microns) at a 5-km horizontal resolution. The 6-hourly horizontal wind fields and CWV from ECMWF interim are available at 0.75° resolution.

### *2.2 Method of defining extreme rainfall systems over the tropics*

We use a system-based method to define extreme rainfall, and the procedure is summarized by the flowchart in Fig. 1. First, the orbital data from PR are remapped into regular longitude–latitude grids at a resolution of 0.1° by 0.1°. We define rainy pixels as any pixel with PR near-surface rain rate over 0.5 mm $h^{-1}$. Spatially contiguous rainy pixels are connected to form rainy systems by applying the four-way connected algorithm in Tsai and Wu (2017) and Chen and Wu (2019). Lastly, the LIS flash counts in the same orbit are colocated with the rainy systems. We also store the system size (square root of horizontal areal coverage), maximum rain rate, and flash counts of the rainy systems, as well as their observation local time and geolocation (geometric center). Systems with a size smaller than 11 km (less than 0.1°) are excluded. Note that the rain rate threshold of 0.5 mm $h^{-1}$ is based on PR's minimum available reflectivity, which is about 17 dBZ. A sensitivity test on the rain rate criteria (0.1, 0.3, 0.5, 0.7, and 0.9 mm $h^{-1}$) was performed, and although the threshold slightly influences the statistics of system size, the choice of rain rate does not affect the major conclusions in this study. Besides, a system may be detected more than once if it lasts sufficiently long and is resampled by multiple 2A25 orbital overpasses. We have examined the occurrence of consecutive detection in our database. Only a few vortex-type systems exhibit such a situation, and they are detected only twice at most.

The thresholds for extreme systems are determined by the 99.9th percentile of all rainfall systems in the tropics, which corresponds to 271 km in horizontal scale and 60.7 mm $h^{-1}$ in maximum rainfall. By applying this definition, 3457 extreme rainfall systems are identified in the tropical regions (30°S–30°N) during years 1998–2014, which account for 0.015 % of total rainy systems. The spatial distribution of these systems is shown in Fig. 2. They occur more frequently near the coastal regions such as the coastline of East Asia, Bay of Bengal, Maritime Continent, Panama, and coastlines of Argentina, and the distribution is

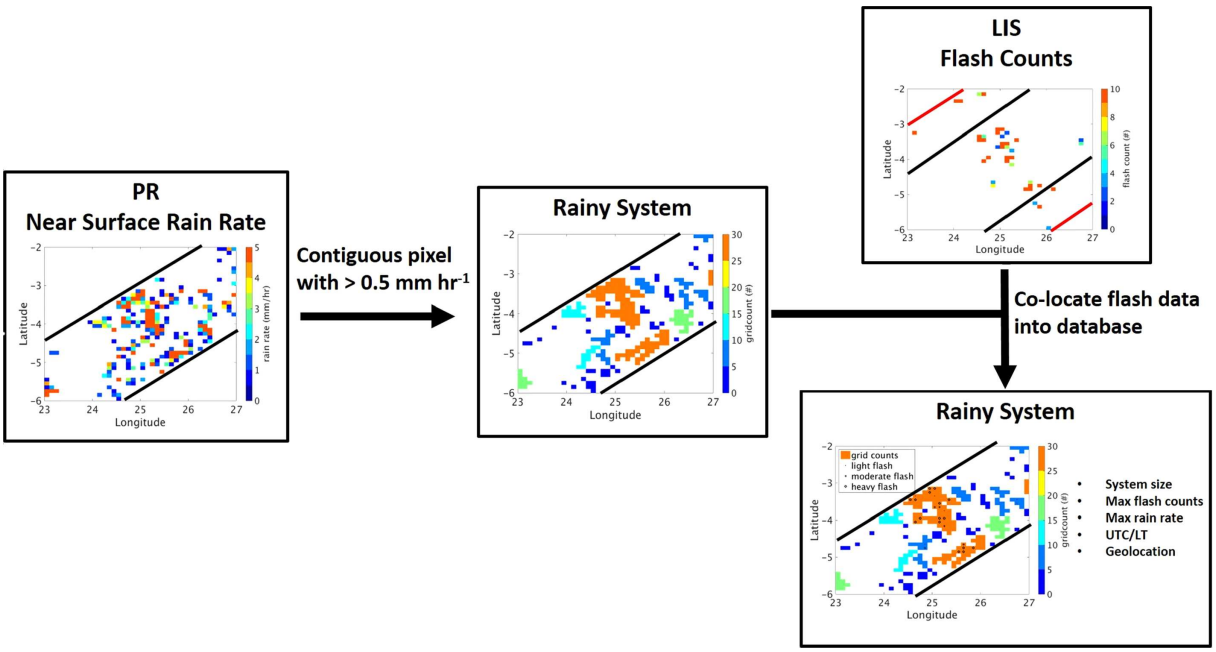


Fig. 1. Flowchart of defining rainy systems in this study. The resolution is 0.1° × 0.1°. The parallel black (red) lines represent the orbital scanning edges of the TRMM PR (LIS). For each rainy system, characteristics such as size, mean rain rate, maximum rain rate, observation time, and geolocation are recorded.

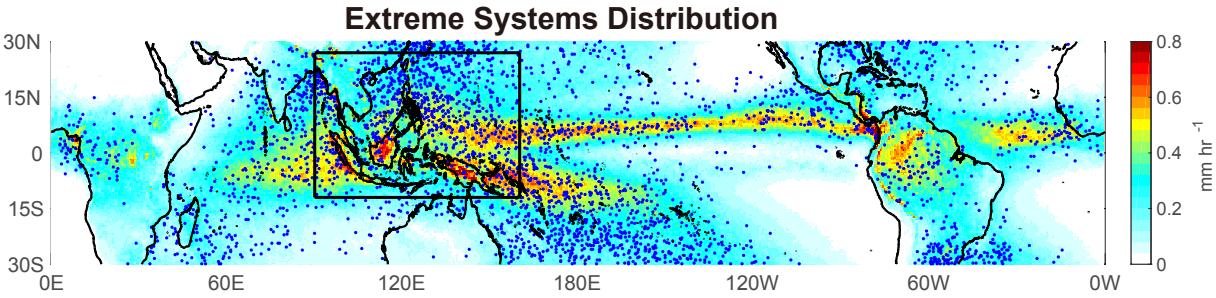


Fig. 2. Location of the extreme rainy systems (blue dot) and annual mean rain rate from PR 2A25 (shading). The domain for analyzing weather states over the Asian-Australian monsoon area is shown by the black box (90–160°E and 12°S–27°N), which encircles 916 extreme systems (27.8 % of total extreme cases over the tropics).

consistent with those reported in previous results (Zipser et al. 2006; Hamada et al. 2014; Liu et al. 2008a; Houze et al. 2015). Of these extreme systems, 85.51 % occurs over water, including coasts, oceans, and lake regions. A total of 916 extreme systems are located over the Asian–Australian monsoon region (90–160°E, 12°S–27°N, black box in Fig. 2), the area of interest in this study. Figure 3 shows the time series of extreme system numbers in the Asian–Australian monsoon region from 1998 to 2014. The annual total number (black line) exhibits two peaks, namely, in 2005 and 2009. The peak in 2009 may result from the numerous TCs in that year (Choi et al. 2015). The linear trend of extreme event number is +0.76 $yr^{-1}$ with a 99 % significance level. Seasonal counts show that most of the extreme systems occur during boreal summer (April to September, red line). There is no significant interannual variation in boreal winter counts, with about 12 extreme systems per season on average. Thus, the year-to-year variation of the annual total is mainly contributed by the interannual variation in boreal summer counts.

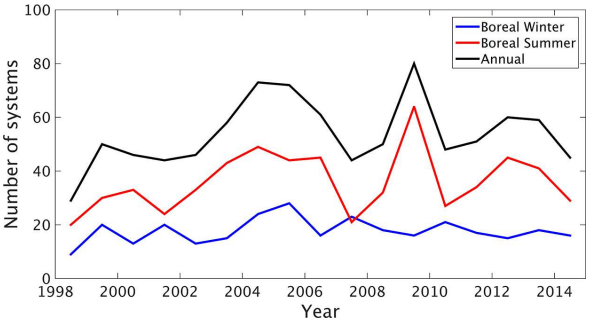


Fig. 3. Time series of extreme system numbers accumulated annually (black) and seasonally (blue for boreal winter and red for boreal summer in the Asian-Australian region).

In the literature on regional extreme events, the features of the extreme events can vary significantly by region (e.g., Hamada et al. 2014). Events in the Asian coastal regions show higher rain rates and larger system sizes for those extreme events, and those in the open ocean show similarly large sizes but relatively low maximum rain rates. The 99.9th percentile over the Asian–Australian monsoon region is 259 km for system size and 65.8 mm $h^{-1}$ for maximum rainfall, only slightly smaller than the threshold over the whole tropics mentioned above (271 km and 60.7 mm $h^{-1}$). Only 42 out of the 916 events will be excluded with the regional thresholds, and it will not significantly change our results. In this study, we aim to investigate the common features of synoptic flows associated with the most intense precipitation systems in the tropics. Therefore, in the next section, we will examine selected case studies and associated classification of synoptic patterns for these 916 extreme systems identified using the whole-tropic thresholds.

## 3. Results

### *3.1 Case studies*

Here, we choose two extreme events to investigate their environments and mesoscale structures in detail. The first event occurred on the west coast of Luzon island on July 31, 2011. The synoptic-scale low-level flow, rainfall, and cloud distribution are shown in Fig. 4a. Rainfall greater than 1 mm $h^{-1}$ was widely spread over the west coast of Luzon island. At the same time, TC Muifa was located about 1000 km away from the east coast of Luzon island. Similar to the scenario conducted from Bagtasa (2019), the circulation of TC Muifa intensified the westerly wind, which brought a high concentration of moisture (high moisture flux) to the northwest of Luzon island, was blocked by the topography of the island, and then eventually induced heavy rainfall. An area of low CTT occurred over Luzon island and extended westward to the South China Sea. Over the east coast of the island, low CTT with no significant precipitation should be cirrus of TC Muifa. On the contrary, low CTT with a wide range of precipitation shows that this event is well developed and organized. On the basis of the PR estimation, the maximum instantaneous surface rain rate of this system reaches 63.15 mm $h^{-1}$, which occurs at about 150 km offshore (Fig. 4b). The inset of Fig. 4a also shows that this event occurred in a moist environment (averaged CWV = 62.83 mm) with averaged vertical wind shear of 1.94 m $s^{-1}$ $(100\ \text{hPa})^{-1}$ [with a broad area of > 2 m $s^{-1}$ $(100\ \text{hPa})^{-1}$].

The mesoscale structure of this system can be examined using the vertical profile of radar reflectivity in Fig. 4c, which shows a cross-section through the latitude where the maximum PR surface rainfall occurs. The highest 30-dBZ echo top, which is associated with the convective part of this system, reaches 10 km (between 118°E and 118.5°E). To the east of this convective part is the broad stratiform area with a lower and less varied echo top height around 5.5 km. The most intense near-surface rain rate is located at the boundary of the stratiform and convective regions.

The three-dimensional structure of this system reveals that the southwest part is the main convective area with a large rainfall rate associated with the well-organized structure. The rain rate generally decreases from the southwest to the northeast, and the vertical extent is not as deep. The broad stratiform rainfall area covers about 100 km off the Luzon island.

Another extreme case is at the northern South China Sea on November 7, 2011 (Fig. 5). Similarly, there was a tropical depression (TD) at the southwestern South China Sea near Indochina, and its circulation enhanced the low-level southerly over this region (Fig. 5a). The 3B42 product shows a broad rainy area extending from 117°E to 122°E over this region and so does the low CTT from MODIS. The southerly winds are enhanced by the TD circulation and then confluence with the low-level easterly wind over the northeast side of the rainy system. For the extreme itself, the maximum rain rate is over 80 mm $h^{-1}$, and the rainy area is over 140000 $km^2$ (Fig. 5b). The most intense region is in the southwest part of the event, and the rainy area extends to the east coast of Taiwan. The average CWV over the event surrounding area is 60.47 mm, and the average low-level vertical wind shear is 3.45 m $s^{-1}$ $(100\ \text{hPa})^{-1}$. Besides, the region with vertical

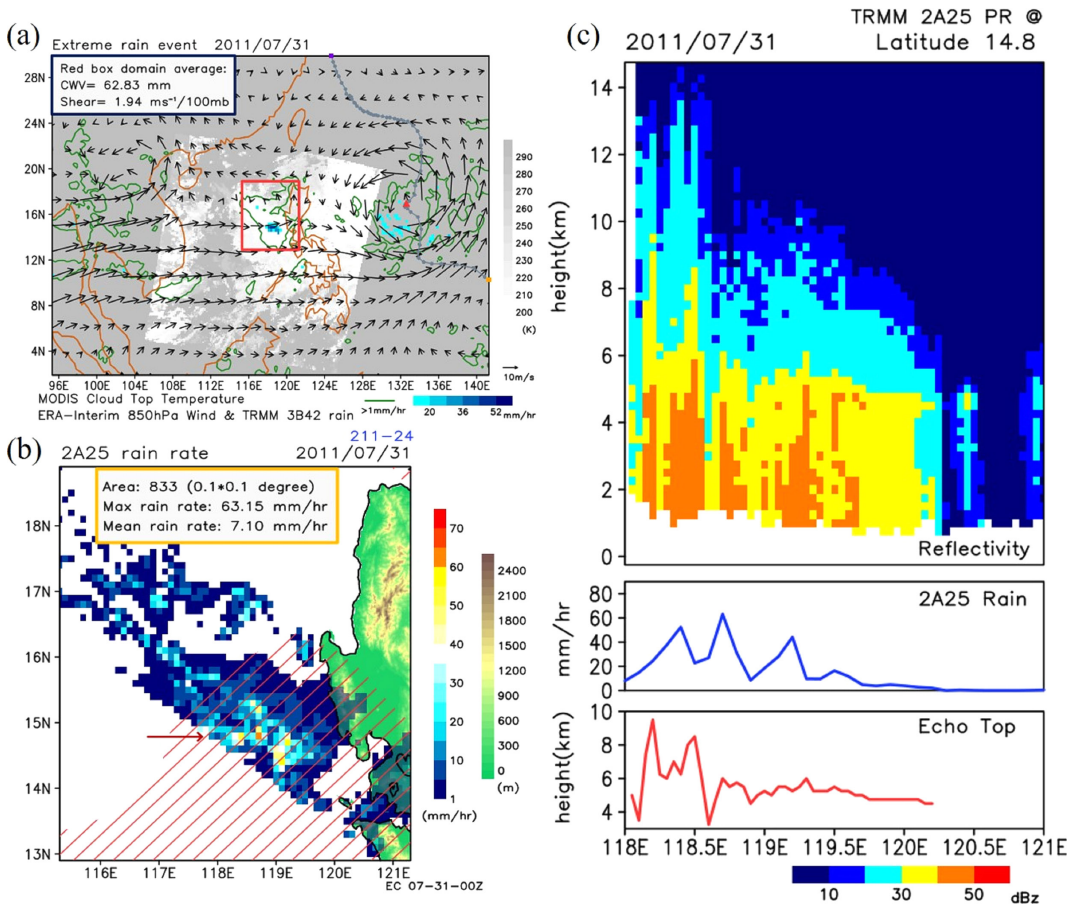


Fig. 4. (a). The ERA-Interim 850 hPa wind field (vectors), 3B42 precipitation rate (green contour and blue shading), Terra MODIS cloud top temperature (grey shading), and the track of TC Muifa around 00Z July 31, 2011. The domain average of the red box region is shown in the left top of the figure. (b). PR 2A25 near-surface precipitation (color shading) over the red box in (a) for the extreme system. Red hatching represents area with vertical wind shear exceeds 2 m $s^{-1}$ (100 hPa)$^{-1}$ between 1000 hPa and 850 hPa, same as in Tsai and Wu (2017). The green-brown shading shows the terrain height over land. The area (i.e. total number of 0.1° × 0.1° grids) and the maximum and mean rain rate of the extreme system are shown in the upper left. (c). The upper panel shows the vertical cross-section of 2A25 radar reflectivity (in dBZ) along the latitude where the maximum near-surface rain rate occurs (14.8°N, marked by the brown arrow in (b), between 118–121°E) in the extreme system. The middle and lower panel shows the 2A25 near-surface precipitation and 30-dBZ echo top, respectively, along the cross-section.

wind shear > 2 m $s^{-1}$ (100 hPa)$^{-1}$ (i.e., the favorable environment for convection organization reported in Tsai and Wu 2017) covers most of this area, except for the southeast side of Taiwan and Taiwan Strait from 23°N to 24°N.

Figure 5c shows the cross-section across latitude 20.8, and the radar echo shows the significant west–east contrast. There are two separate 40-dBZ echo signals with vertical continuity, which suggests that this rainy event has multiple convective cores. Even though the 30-dBZ echo top height is lower compared with the previous case, which is slightly higher than 6 km, the maximum surface rain rate is more intense. According to the significant drop of rain rate at 118°E and the relatively uniform 30-dBZ echo top heights, the rainfall types over this region are primarily stratiform rainfall.

The above analysis for these two extremes shows some similarities. They both occur in a significant synoptic state that is influenced by a circulation caused by the surrounding TC, and the extreme rain rate occurs in the boundary of convective and stratiform rainfall

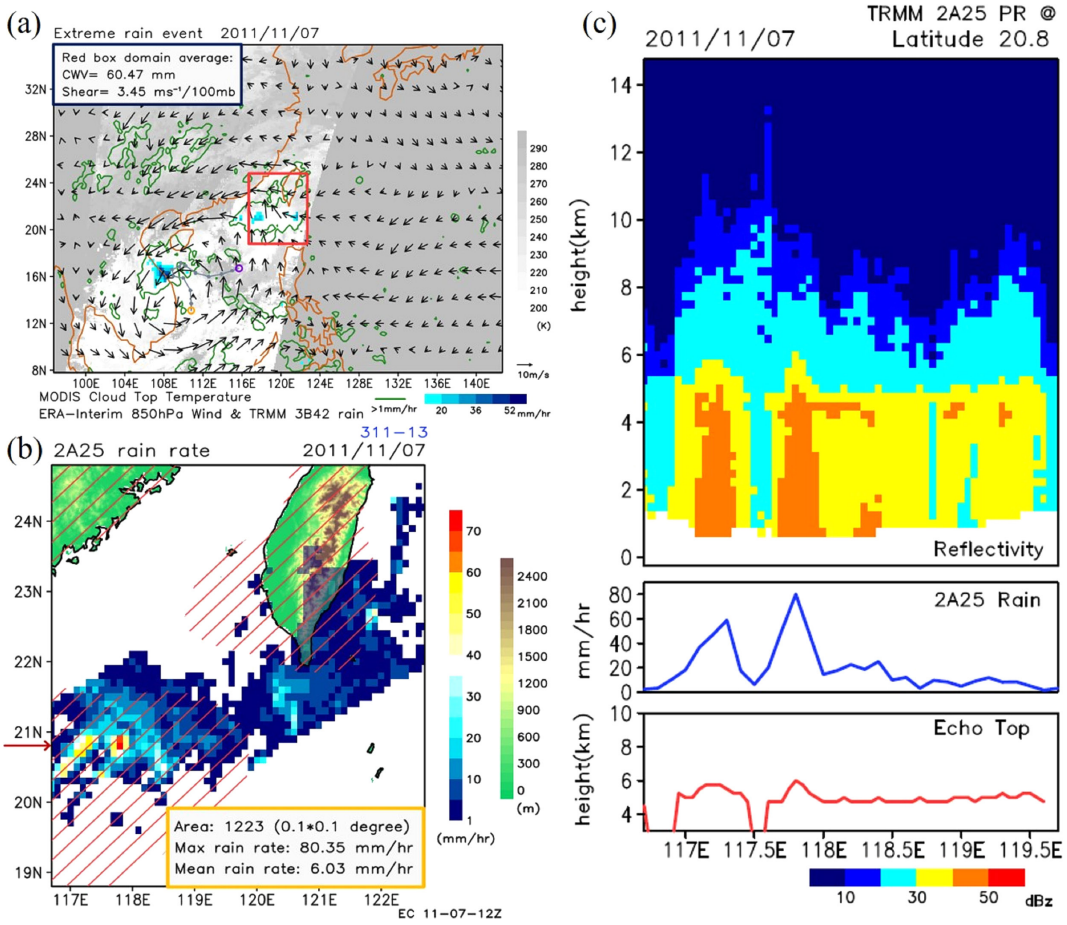


Fig. 5. Similar to Fig. 4 but for the extreme system occurred on November 7, 2011. The grey line in (a) shows the track of the TD. The size and rain rate statistics of the extreme system is shown in the lower right in (b). The cross-section in (c) is along 20.8°N.

regions. Whether it is a robust feature for all of the extreme events needs further investigation. On the other hand, the tropical extreme events examined in this study usually involve the multiscale interactions of the topography, synoptic weather system, tropical waves, and seasonal background winds. Even when focusing on a specific location, the pattern and intensity of the synoptic weather or tropical waves can still vary among events. If carrying out composite analyses of the large-scale flow, the signals of the weather will be averaged out, leaving mostly the seasonal or annual mean background. Therefore, in the subsequent analysis, we will examine and classify each event individually for the features of the synoptic-scale flow.

### 3.2 *Classification of synoptic state*

Here, we subjectively label and classify the synoptic states of the 916 extreme systems over the Asian–Australian Monsoon region based on the patterns of the ERA-Interim 850 hPa-level circulation and TRMM 3B42 rainfall over a 45° × 28° longitude-latitude area surrounding each event. Four categories are identified, namely, vortex (V), coastal (C), coastal with vortex (VC), and none of above (N). Figure 6 gives examples of these four types, including the synoptic circulation and rainfall distribution (left column) and the detailed surface precipitation within the system from the PR observation (right column). The V type requires the extreme system to be directly embedded in a synoptic-scale cyclonic circulation. The center of the extreme system can be located near the coastal water or open ocean. The circulation of the vortex in this classification can be associated with a TC, tropical disturbance, or synoptic-scale

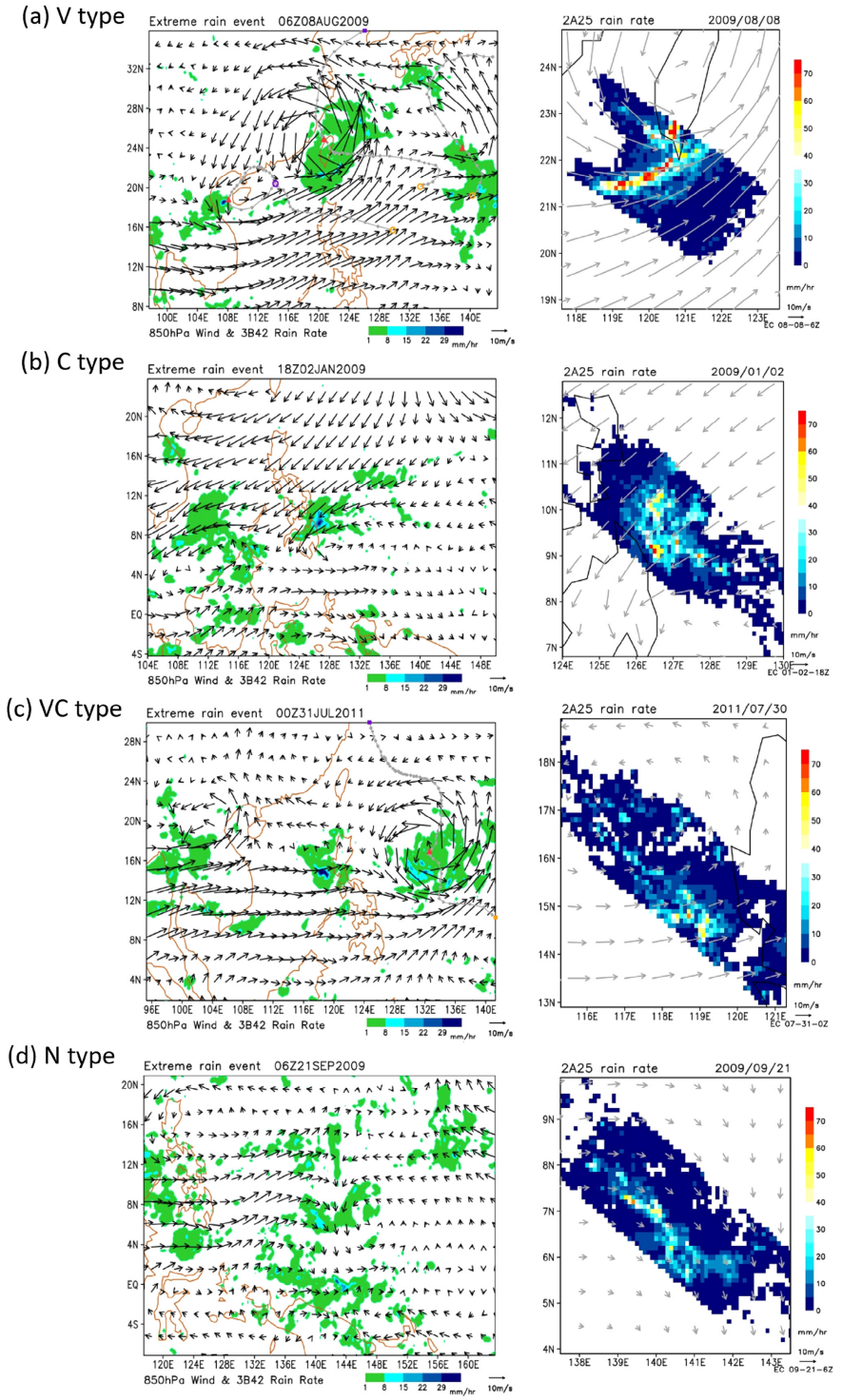


Fig. 6. Examples of different synoptic types of the extreme systems: (a) V-type system near Taiwan on August 8, 2009. The red triangle stands for the current center of a tropical cyclone (Morakot). (b) C-type system in the south of the Philippines on January 2, 2009. (c) VC-type system at the west of Luzon Island on July 31, 2011. (d) N-type system in the Pacific Ocean on September 21, 2009. The detailed precipitation characteristics are presented on the right-hand-side figure.

tropical waves. Figure 6a shows the example of the V type, with Typhoon Morakot near Taiwan. This typhoon caused intense rainfall and landslides in the south of Taiwan and a significant loss of life during the landslides. The C type requires the center of the extreme system to occur within 2.5° offshore, without the presence of synoptic-scale cyclonic circulations in the surroundings. Figure 6b shows a C type over the southern Philippines. The onshore synoptic-scale northeasterly made the coastal convection sustained and developed in this case. The VC type also requires the extreme system to be offshore as the C type, and the onshore wind is enhanced by a nearby synoptic-scale vortex, but the rainfall of the extreme system is not directly associated with the vortex circulation. Such an example can be seen in Fig. 6c, when TC Muifa was located about 1000 km from Luzon island, Philippines. The onshore westerly wind over the South China Sea to the coast of Luzon island is enhanced, and an extreme system with maximum rainfall over 63 mm $h^{-1}$ occurs near the coastline. The N type involves extreme systems located over the open ocean without the circulation of a synoptic vortex (Fig. 6d), and they are mainly associated with tropical disturbances without a prominent cyclonic circulation or frontal system. Figure 6d shows an N-type example located in the open Pacific Ocean with no significant synoptic-closed circulation near the extreme system.

Table 1 shows the percentage of the four synoptic types for the 916 extreme systems. Even though the percentage of the V type is the highest, the percentage is only 43.9 %, less than half of the total systems. A TC accounts for 93.9 % of total V-type extreme systems. The percentage of C type is 29.3 %, the second frequent type in our database. The VC and N types account for 7.2 % and 19.7 %, respectively. The percentage of the VC type is low but not negligible.

The occurrence of the synoptic types associated with the extreme precipitation systems is highly related to the monsoon season. Figure 7 compares the spatial distribution of each type in boreal summer (April to September, red dots) and boreal winter (October to March, blue dots). The V-type events mainly occur in boreal summer and are distributed at off-equatorial areas (north of 10°N), including the South China Sea, Pacific Ocean, Philippines, Taiwan, and the coast of Vietnam (Fig. 7a), as the higher planetary vorticity provides a favorable condition for vortex generation. The number of C-type events is similar in boreal summer and winter, but the locations vary significantly with the season (Fig. 7b). In boreal summer, most systems occur over the Bay of Bengal and the coastal region surrounding the South China Sea. On the other hand, in boreal winter, they mainly occur on the west coast of Sumatra and Borneo. In addition, in the deep tropics, the C-type events more frequently occur in boreal winter compared with the other types. The occurrence of the VC-type event is located in specific regions, and systems occur west of the Asian–Australian Monsoon region such as coastal regions near the South China Sea in boreal summer and east of the region such as west of Borneo and the coastal region near New Guinea in boreal winter (Fig. 7c). Since vortices mainly occur in the Northwest Pacific and propagate to Northeast Asia, the VC type, which is highly related to the topography and flows from the vortex nearby, occurs west of the islands in boreal summer such as the west coastline of the Philippines, Burma, and Borneo. Lastly, most of the N-type events occur over the open ocean, especially in the Pacific (Fig. 7d). Seasonal variability of the events is weak in the equatorial Pacific region, but in higher latitude regions, the N-type events mostly occur in boreal winter, and these systems are mainly associated with the extratropical front.

Table 1. Percentage of the synoptic types of the extreme systems in the Asian-Australian monsoon region from 1998 to 2014, and the probability of their association with lightning flash. Abbreviations: V = vortex system; C = coastal convections; VC = coastal convections with vortex nearby; N = none of the above.

| Type | Percentage | Flash probability |
|---|---|---|
| V | 43.9 % (402/916) | 0.41 |
| C | 29.3 % (268/916) | 0.54 |
| VC | 7.2 % ( 66/916) | 0.56 |
| N | 19.7 % (180/916) | 0.35 |

### *3.3 Characteristics of extreme rainfall systems*

In general, rainfall in the tropical coastal areas exhibits strong diurnal variations (Zhou and Wang 2006; Takahashi et al. 2010), with exceptions such as the regions of western India (Western Ghats) and Myanmar (Shige et al. 2017). The occurrence of extreme rainfall systems, particularly near the coastal areas, may therefore also be associated with diurnal cycle processes. Here, we examine the diurnal cycle (DC) of occurrence for each synoptic type of extreme systems, as shown in Fig. 8. The statistics are based on 3-hourly time windows in local time (LT) to guarantee enough sample sizes. All, except the V type, exhibit more frequent occurrence during late night to early morning (01–09 LT) than in the afternoon

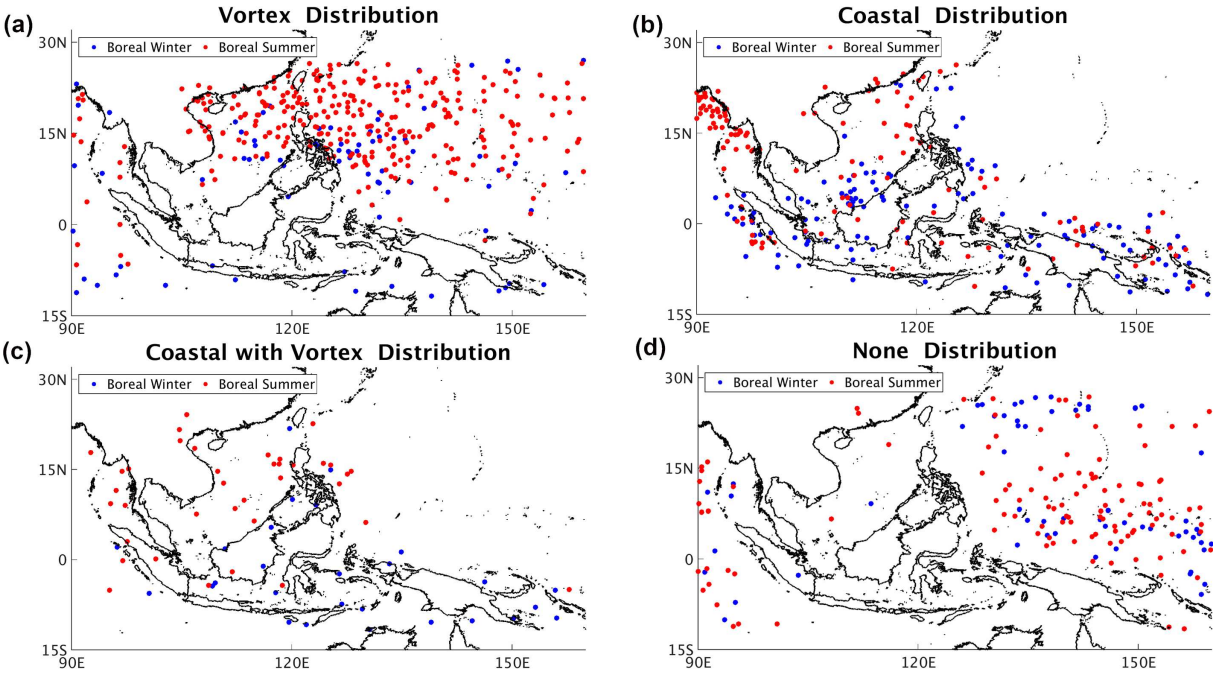


Fig. 7. Spatial distribution for extreme rainy systems in boreal summer (red dots) and boreal winter (blue dots) for (a) V, (b) C, (c) VC, and (d) N types. The dot marks the geometric center of each system.

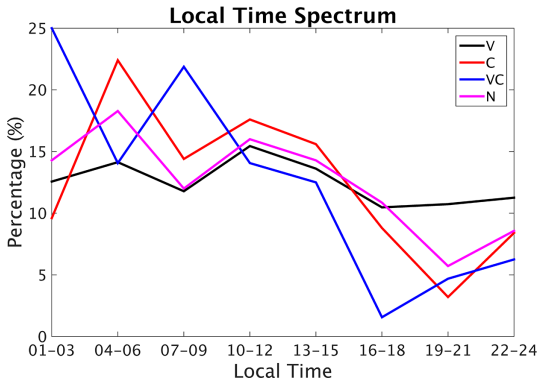


Fig. 8. Diurnal variation of occurrence for different types of extreme systems.

to late evening (16–24 LT). Previous observational studies based on TRMM satellite data showed that the mean rainfall DC over coastal regions, in general, exhibits an early morning peak at 05 LT (Takahashi et al. 2010; Hirose et al. 2017b). These early morning coastal convective systems are associated with long-lasting rainfall events with high intensity. The extreme rainfall systems defined in this study are both intense and large. The consistency between the DC peak time of the coastal mean rainfall and the DC of occurrence for the C and VC types suggests that these systems are more likely associated with the long-lasting events, instead of the short-duration intensive events that mostly occur in afternoon thunderstorms over land. The N-type events, which are mainly located over the open ocean, also show high occurrences from midnight to early morning. The mean rainfall DC over the tropical open ocean, in general, shows a nocturnal peak hour, and the amplitude of DC is weak compared with the coastal and land areas (Romatschke et al. 2010; Liu 2011; Liu et al. 2008b). This nocturnal signal is attributed to the radiative cooling that leads to the destabilization of the atmosphere in the nighttime and moistening the mid-level atmosphere (Sui et al. 1997). Other mechanisms, such as the direct cloud–radiation interaction and the cloud–cloud-free differential heating, may also play a role (Liu and Moncrieff 1998). Whether the above mechanisms also control the development of extreme rainfall requires more investigation in the future. Lastly, the V type shows an insignificant diurnal occurrence, indicating that solar heating may not be the major control of the development of these extreme systems, and the other factors, such as vortex dynamics, might play a more crucial role.

The occurrence of lightning is often regarded as a metric for the intensity of convective systems. Previous studies on the distribution of lightning flashes showed a great land–sea contrast (Boccippio et al. 2002; Cecil et al. 2005; Zipser et al. 2006) with a higher probability of lightning over land. In our dataset, only 1 % of tropical rainfall systems exhibit flashes, and most of these systems occur over land. Table 1 shows the probability of each synoptic type in the Asian–Australian Monsoon area to be associated with lightning flashes, and the numbers for these extreme systems are predominantly higher than the general tropical systems. The C and VC types are most likely to exhibit flashes, with probability values of 0.54 and 0.56, respectively. The probability values of flash are only 0.41 and 0.35 for the V type and N type, respectively.

The probability distributions of the maximum rain rate and system size are shown in Fig. 9. The median of the maximum rain rate is similar among the four types (72 mm $h^{-1}$). On the other hand, the variability of the maximum rain rate is greatest for the V-type systems, with the highest values exceeding 140 mm $h^{-1}$. The C type has the second highest maximum rain rate value (> 120 mm $h^{-1}$). The VC and N types show similar variability values in the maximum rain rate. As TRMM PR usually samples the TCs only partially, the large variation of the maximum rain rate in the V-type systems may result from different structures within a TC, such as intercore rainband and outer rainband, more likely than from TCs of various intensity. For system size, the N type is slightly larger (median, 320 km; highest value, over 430 km), whereas the other types of extremes exhibit a similar horizontal scale around 300 km. The larger system size for N-type extremes may be due to their association with frontal systems.

## 4. Discussion

The seasonal-spatial distribution in Fig. 7 shows distinct hotspots of occurrence for C and VC synoptic types of the tropical extreme rainfall systems. In boreal summer, the C type (Fig. 7b) occurs much more frequently in the Bay of Bengal than other coastal regions at similar latitudes, such as Taiwan and southeast China. The VC type mostly occurs on the coastal regions near the South China Sea in boreal summer and the west of Borneo and the coastal region near New Guinea in boreal winter (Fig. 7c). Previous studies have found that the development of convective systems in the Bay of Bengal is highly related to sea surface temperature (SST), wind direction, and

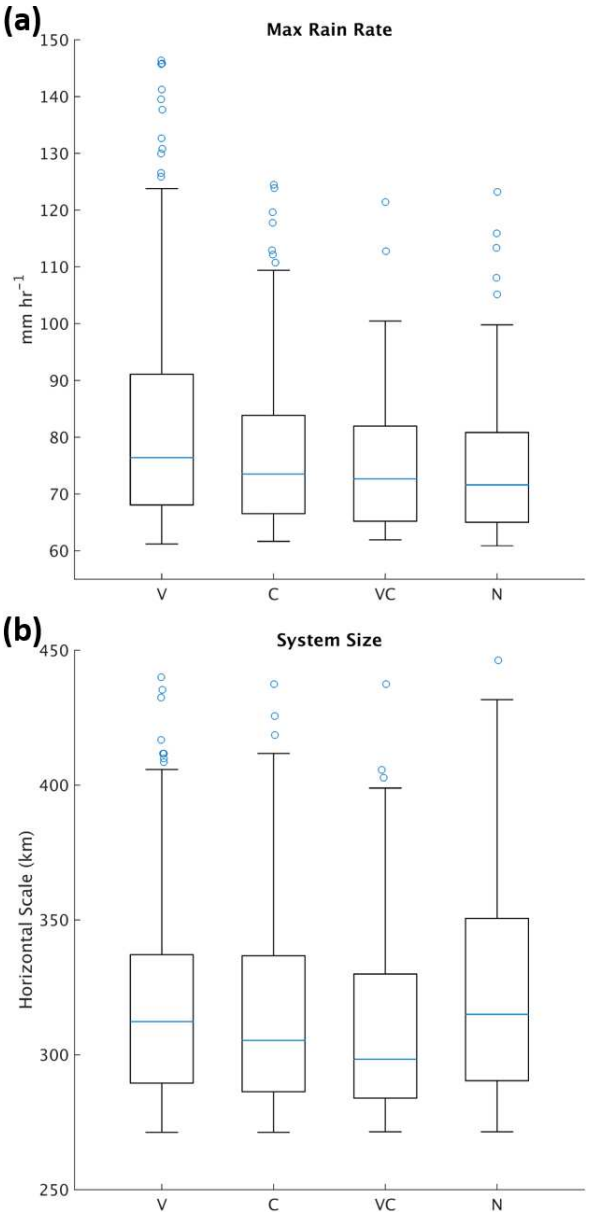


Fig. 9. Box plot of the maximum rain rate (a) and system size (b) of different types of extremes. The blue horizontal line represents the median value, the upper (lower) part of the box is 75th (25th) percentile. The maximum and minimum are defined as 1.5 IQR (Interquartile Range) extending from the box. The blue cycles are the outliers.

topography, particularly in summer monsoon season (Kilpatrick et al. 2017; Jain et al. 2018; Zuidema 2003; Liu et al. 2008). The warm SST and abundant water vapor in the lower atmosphere create an unstable environment. Topography blocks and lifts the onshore winds, along with the land–water diurnal heating contrast, which promotes the genesis of convective systems over the coast. As onshore wind keeps blowing or even enhances, these coastal convective systems can grow and develop into organized rainfall systems (Xu et al. 2012), and they will have a higher probability to produce extreme rainfall. The enhanced and persistent onshore wind can result from synoptic-scale circulations such as large-scale monsoon flow or synoptic vortices. According to Tsai and Wu (2017), aggregation of rainfall systems is related to sufficient water vapor and proper wind shear. To explore the potential environmental conditions for the C and VC types, we analyzed the seasonal climatology of the frequency of high total column water vapor (TCWV) and low-level wind shear (wind difference between 1000 and 850 hPa) in the region of interest. The frequency of both daily TCWV exceeding 57.6 mm (the 75th percentiles) and the wind shear exceeding 2 m $s^{-1}$ (100 hPa)$^{-1}$ during 2001–2014 is shown in Fig. 10. Regions of high occurrence (> 40 %) of the favorable environment for organized convection are mainly near the coastal areas, with a significant seasonal variation. Even though there are few extreme events that occur at the relatively low TCWV and weak wind shear regions, such as east of Taiwan and the Philippines, most of the location is highly consistent with the seasonal-spatial distribution of the C and VC types. The wind shear near the coast might be related to the low-level jet, which provides another mechanism to sustain or even enhance this rainfall system (Xu et al. 2012).

On the other hand, the environment for the C type near Sumatra and Borneo in boreal winter is different. As some of the strong northeasterly cold surge events intrude southward into the deep tropics, they can trigger the moisture transport, provide additional terrain-blocked convergence and wind shear, and sometimes interact with the MJO to enhance the development of the Borneo vortex and coastal convection (Lim et al. 2017; Wicaksono and Hidayat 2016).

The case studies in Section 3.1 of the two extreme systems showed that both systems exhibit a wide convective region and a broad stratiform region, and the maximum rain rate occurs near the boundary of the convective and stratiform part. To further examine the internal vertical structures of the extreme systems

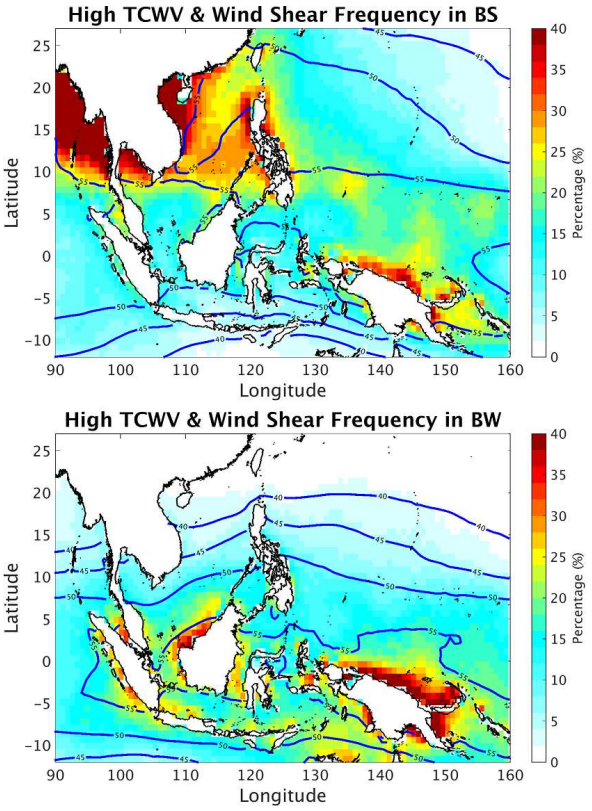


Fig. 10. Occurrence frequency (shading) of exhibiting both high TCWV (daily mean > 57.6 mm; 75th percentiles over the analyzed domain) and moderate low-level wind shear (if any of the four 6-hr reanalysis data in a day > 2 m $s^{-1}$ (100 hPa)$^{-1}$ between 1000 hPa and 850 hPa in boreal summer (upper) and boreal winter (bottom) based on TRMM TMI and ERA-Interim over 2001–2014. The mean TCWV in each season is shown by the blue contour.

in the present study, we collocate our database with the classification of convective systems associated with the lifecycle of organized convection and MCSs (Houze et al. 2015; Rasmussen et al. 2015), in which the structures of rainfall systems are identified as Deep Convective Core (DCC), Wide Convective Core (WCC), Deep Wide Convective Core, Broad Stratiform region (BSR), and Shallow Isolated based on the TRMM PR radar echo. Note that the overlapped period is from 1998 to 2013 and the overlapped area in the warm pool region is 90–150°E, 12°S–27°N. The overlapped data yield a total of 760 extreme cases (out of the original $n$ = 916), and their statistics are shown in Table 2. The extreme systems in this study

Table 2. Percentage of the various mesoscale structures defined in Houze et al. (2015) in each synoptic type of the extreme systems. The overlapped period and regions between our data based and the Houze et al. (2015) data covered a total of 760 extreme cases.

| Type | Deep Convective Core | Wide Convective Core | Deep Wide Convective Core | Broad Stratiform |
|---|---|---|---|---|
| V | 0.7 % | 46.4 % | 1 % | 51.8 % |
| C | 0 % | 55.9 % | 0.3 % | 43.7 % |
| VC | 0 % | 51.8 % | 0 % | 48.2 % |
| N | 0 % | 48.4 % | 0 % | 51.6 % |

mostly exhibit the WCC and BSR structures. Rasmussen et al. (2015) showed that near the coast in the Asian–Australian Monsoon region, including the Bay of Bengal, the Philippines, and Sumatra, the WCCs account for 5–10 % of the total identified convective systems and the BSRs contribute to another 15–35 %. The hotspots of occurrence of the WCC and broad stratiform systems are highly consistent with the hotspots of the C and VC types of synoptic pattern in this study. The results indicate that systems with these two types of internal structure are more likely to be associated with extreme rainfall. In Table 2, the fraction of the DCC systems (highest 40-dBZ echo > 10 km) is relatively low. One reason is that the DCCs mainly occur over land, and the present study only considers the extreme rainfall systems over coastal water and open ocean. In addition, a recent study showed a weak linkage between the heaviest rainfall and tallest storms in the tropics from TRMM's observations (Hamada et al. 2015), which also explains why the DCC fraction is low in our extreme systems. On the other hand, Gingrey et al. (2018) pointed out that the height of deep convection may be underestimated by the Ku-band TRMM PR when compared to the ground-based S-band radar. Our statistics here showed that tropical extreme rainfall systems, in general, exhibit a wide convective part and a BSR with the highest 40-dBZ radar echo lower than 10 km. In the future, reflectivity from the Dual frequency PR (Ku- and Ka-bands) onboard the Global Precipitation Measurement Core Observatory can be analyzed to confirm these features of the internal structure in tropical extreme systems.

To investigate whether the maximum rain rate occurs near the boundary between convective and stratiform regions in the precipitation system, we combined the extreme events with the two-dimensional ($x$–$y$) rain-type (convective/stratiform) mask from the gridded (0.05°) 2A23 dataset of Houze et al. (2015). Note that only extreme systems with the rain type of the maximum rate identified as convective or stratiform are chosen. The rain-type identification algorithm (Awaka et al. 2009) mainly considers the vertical radar echo shape (V-method) and the localized reflectivity relative to the surrounding environment (H-method). The rain type would be determined as stratiform when the bright band is detected in the single vertical reflectivity profile. In addition, if the maximum radar reflectivity (Z) occurs below the estimated freezing level and Z is below 40 dBZ, the rain type would also be recognized as stratiform (V-method). On the other hand, if Z at a specific pixel exceeds 40 dBZ or is sufficiently higher than the horizontally averaged Z over its surroundings, the rain type would be classified as convective (H-method). Figure 11 shows the examples of the rain-type mask for four types of extreme along with their rain rate distribution and the location of maximum rainfall within each system. The maximum rain rate of the V synoptic-type example occurs in the stratiform region (Fig. 11a), and those of the C-, VC-, and N-type examples occur in the convective region (Figs. 11b–d). Moreover, the maximum rain rates in all four examples are located near the boundary between the convective and stratiform regions. By selecting the extreme rainfall systems with the rain type of the maximum rain rate recognized as convective or stratiform, 650 extreme systems are considered in the statistics of Table 3. About 70 % of the maximum rain rate is in the convective area of the precipitation system, and the other 30 % is in the stratiform area. The percentage is similar across different synoptic types. The distance between the maximum rain rate pixel and nearest convective–stratiform boundary is also calculated for each system, the median value is 5.5 km, and in 90 % of the extreme rainfall systems, the maximum rainfall occurs within 11 km to the convective–stratiform boundary.

Our result of about 70 % of the extreme systems with maximum rainfall as convective is lower than the percentage of 95 % reported in Hamada et al (2015). Such differences may be related to the different selection of extreme systems between the two studies. In the present study, thresholds for extreme rainfall systems are defined from the tropical wide range samples, and Hamada et al. (2015) defined the thresholds at each 2.5° × 2.5° local grid. Additionally, the extreme thresholds in this study are based both on system size and on the intensity of the maximum rain rate, and those by Hamada et al. (2015) are based on their maximum near-surface rainfall rates. The rainfall systems

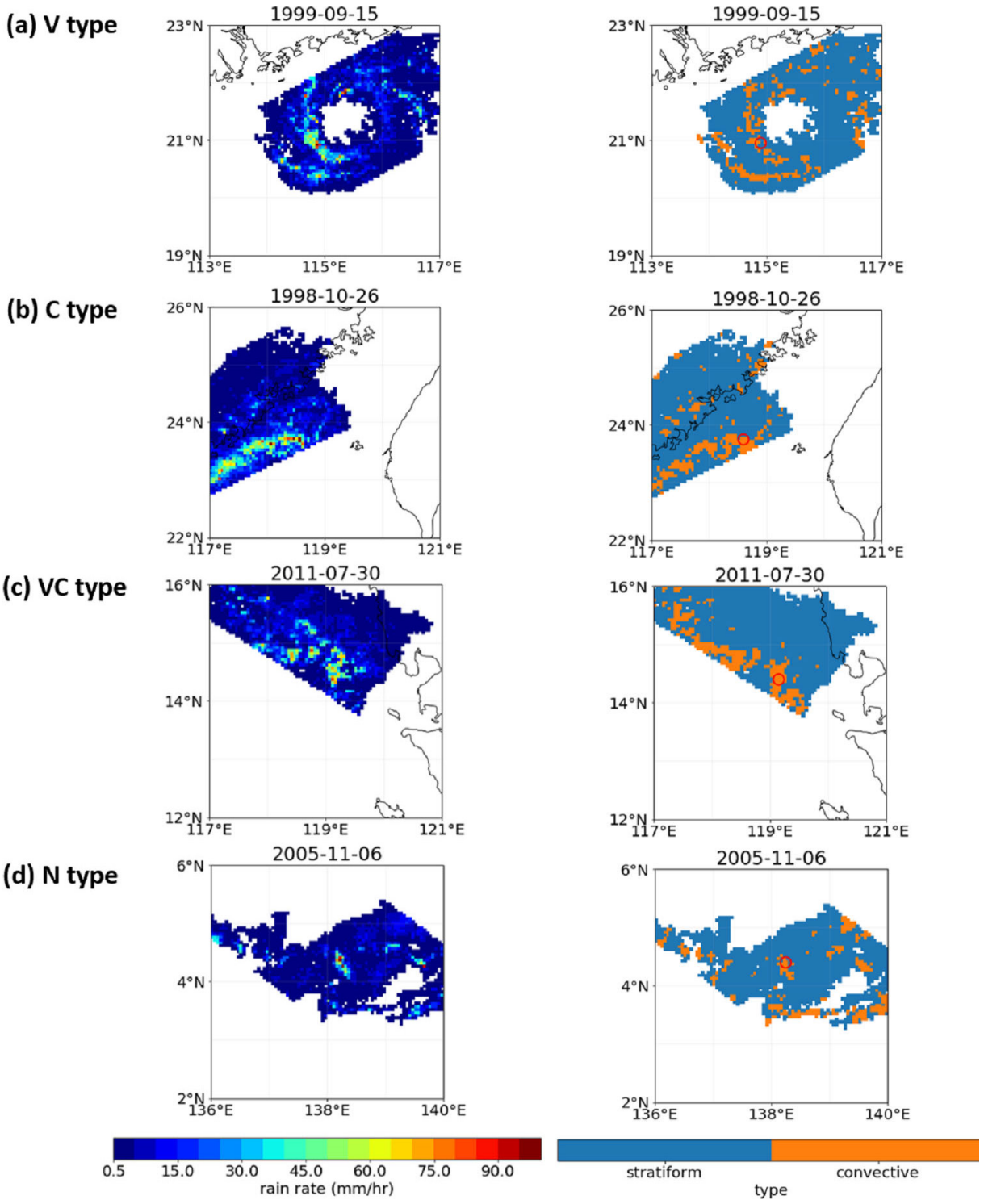


Fig. 11. Examples showing the location of maximum rainfall and the corresponding rain type in extreme systems selected from different synoptic types: (a) V, (b) C, (c) VC, and (d) N types. The left column shows the rain intensity distribution from TRMM 2A25. The right column shows the rain type from TRMM 2A23 of stratiform (blue) and convective (orange) region. The red circle marks the pixel of the maximum rain rate in each system.

Table 3. Percentage of the location of maximum rain rate within the convective or stratiform area of the extreme systems for each synoptic type. The statistics are based on 650 extreme cases in which the maximum rain rate is recognized as convective or stratiform by the 2A23 rain type algorithm.

| Synoptic Type of Extreme | Maximum rain in Convective Area | Maximum rain in Stratiform Area |
|---|---|---|
| V | 62.7 % (185/295) | 37.3 % (110/295) |
| C | 70.4 % (138/196) | 29.6 % ( 58/196) |
| VC | 65.3 % ( 32/ 49) | 34.7 % ( 17/ 49) |
| N | 72.7 % ( 80/110) | 27.3 % ( 30/110) |

with extremely large size focused in our study usually consist of both convective and wide stratiform regions (Table 2). Despite a higher percentage (~ 30 %) of maximum rainfall as stratiform in these systems, they are still very close to the convective part. One possibility is that some of these systems exhibit tilting updraft cores, especially in an environment with vertical wind shear (Xu et al. 2012). The tilting structure may lead to a less pronounced horizontal gradient of radar reflectivity, or the strongest reflectivity is not directly above the heaviest near-surface rainfall. In the future, the radar echo profiles near the maximum rain rate and the internal structures of these extreme systems should be further investigated in detail.

## 5. Summary and conclusion

This study identified the major types of synoptic flow patterns associated with extreme rainfall over the Asian–Australian monsoon region. The extreme events were defined by a system-based method with the 17-year TRMM PR surface rainfall, with both maximum rainfall and horizontal scale exceeding the 99.9th percentile of all tropical rainfall systems. For a total of 916 extreme systems, the surrounding synoptic winds and rainfall distribution were classified into four major types. The coast-related extremes (C and VC types) accounted for 36 %, and both types showed great seasonal variations. These C and VC types exhibited more frequent occurrences during late night to early morning (01–09 LT), and they were more likely to be accompanied by lightning flashes. The system-based dataset gave advantages to investigating regional climatology and the internal structure of each system. Because we defined the extreme rainfall system by system, the internal structure of the system producing the extreme rainfall can be examined. This enabled us to identify that extreme systems mostly have similar internal structures of WCCs and BSRs. Besides, the maximum rain rate will occur at the boundary of convective and stratiform regions with over 90 % of cases within about 11 km. The analysis of the environment associated with extreme systems with similar structures can therefore be focused on the interactions between the specific synoptic state and the topography or coastlines around the occurrence hotspots. Our results highlight the importance of the strength and direction of the synoptic flow for the development of extreme rainfalls over the tropical/monsoonal coastal areas exhibiting seasonally high moisture. The land–sea breeze and diurnal cycle of convection over the nearby land provide regular diurnal initiation and enhancement of coastal convection. If the orientation of the topography or coastline can generate or enhance the low-level vertical wind shear under specific synoptic flows, the probability of convective organization will be enhanced. Further analysis on the time evolution of synoptic flows and moisture transport during the occurrence of the extreme systems can be done, but it is beyond the scope of the current study. The moderate wind shear in the Asian–Australian monsoon region could be related to the low-level jet during the summer monsoon. The vertical integral water vapor transport, which combines both dynamic and thermodynamic parameters, may serve as useful guidance for monitoring and nowcasting extreme rainfall over specific coastal areas. It also serves as a key linkage between the mesoscale convective processes and large-scale flow when investigating the response of the extreme rainfall systems in a changing climate.

## Acknowledgment

This work was jointly supported by the Ministry of Science and Technology of Taiwan (MOST108-2111-M-002-004; MOST 107-2111-M-002-010-MY4) and the Central Weather Bureau in Taiwan (1082014C). Co-author Rasmussen acknowledges support from the National Science Foundation grant AGS-1854399. The authors would like to thank Professor Hung-Chi Kuo at NTU for the insightful discussion and comments on the manuscript. The observation and reanalysis datasets were downloaded from the following sources:

- TRMM 2A25 (1998-2015): https://disc2.gesdisc.eosdis.nasa.gov/data/TRMM_L2/TRMM_2A25.7/ (Accessed July 13, 2018)
- TRMM LIS (1998-2015): https://ghrc.nsstc.nasa.gov/hydro/#/orders?mydata=lislip&_k=v7e78a (Accessed December 13, 2016)
- TRMM 3B42 (1998-2015): https://pmm.nasa.gov/data-access/downloads/trmm (Accessed March 21, 2019)

• ERA-Int (1998-2015): http://apps.ecmwf.int/datasets/data/interim-full-daily/levtype=sfc/ (Accessed March 21, 2019)

## References


Awaka, J., T. Iguchi, and K. Okamoto, 2009: TRMM PR standard algorithm 2A23 and its performance on bright band detection. *J. Meteor. Soc. Japan*, **87A**, 31–52.

Bagtasa, G., 2019: Enhancement of summer monsoon rainfall by tropical cyclones in northwestern Philippines. *J. Meteor. Soc. Japan*, **97**, 967–976.

Boccippio, D. J., W. J. Koshak, and R. J. Blakeslee, 2002: Performance assessment of the optical transient detector and lightning imaging sensor. Part I: Predicted diurnal variability. *J. Atmos. Oceanic Technol.*, **19**, 1318–1332.

Cecil, D. J., S. J. Goodman, D. J. Boccippio, E. J. Zipser, and S. W. Nesbitt, 2005: Three years of TRMM precipitation features. Part I: Radar, radiometric, and lightning characteristics. *Mon. Wea. Rev.*, **133**, 543–566.

Chen, Y.-T., and C.-M. Wu, 2019: The role of interactive SST in the cloud-resolving simulations of aggregated convection. *J. Adv. Model. Earth Syst.*, **11**, 3321–3340.

Choi, Y., K.-J. Ha, C.-H. Ho, and C. E. Chung, 2015: Interdecadal change in typhoon genesis condition over the western North Pacific. *Climate Dyn.*, **45**, 3243–3255.

Davis, C. A., and W.-C. Lee, 2012: Mesoscale analysis of heavy rainfall episodes from SoWMEX/TiMREX. *J. Atmos. Sci.*, **69**, 521–537.

Dee, D. P., S. M. Uppala, A. J. Simmons, P. Berrisford, P. Poli, S. Kobayashi, U. Andrae, M. A. Balmaseda, G. Balsamo, P. Bauer, P. Bechtold, A. C. M. Beljaars, L. van de Berg, J. Bidlot, N. Bormann, C. Delsol, R. Dragani, M. Fuentes, A. J. Geer, L. Haimberger, S. B. Healy, H. Hersbach, E. V. Hólm, L. Isaksen, P. Kållberg, M. Köhler, M. Matricardi, A. P. McNally, B. M. Monge-Sanz, J.-J. Morcrette, B.-K. Park, C. Peubey, P. de Rosnay, C. Tavolato, J.-N. Thépaut, and F. Vitart, 2011: The ERA-interim reanalysis: Configuration and performance of the data assimilation system. *Quart. J. Roy. Meteor. Soc.*, **137**, 553–597.

Gingrey, A., A. C. Varble, and E. J. Zipser, 2018: Relationships between extreme rain rates and convective intensities from the perspectives of TRMM and WSR-88D radars. *J. Appl. Meteor. Climatol.*, **57**, 1353–1369.

Goswami, B. B., P. Mukhopadhyay, R. Mahanta, and B. N. Goswami, 2010: Multiscale interaction with topography and extreme rainfall events in the northeast Indian region. *J. Geophys. Res.*, **115**, D12114, doi:10.1029/2009JD012275.

Hamada, A., and Y. N. Takayabu, 2018: Large-scale environmental conditions related to midsummer extreme rainfall events around Japan in the TRMM region. *J. Climate*, **31**, 6933–6945.

Hamada, A., Y. Murayama, and Y. N. Takayabu, 2014: Regional characteristics of extreme rainfall extracted from TRMM PR measurements. *J. Climate*, **27**, 8151–8169.

Hamada, A., Y. N. Takayabu, C. Liu, and E. J. Zipser, 2015: Weak linkage between the heaviest rainfall and tallest storms. *Nat. Commun.*, **6**, 6213, doi:10.1038/ncomms7213.

Hirose, M., Y. N. Takayabu, A. Hamada, S. Shige, and M. K. Yamamoto, 2017a: Impact of long-term observation on the sampling characteristics of TRMM PR precipitation. *J. Appl. Meteor. Climatol.*, **56**, 713–723.

Hirose, M., Y. N. Takayabu, A. Hamada, S. Shige, and M. K. Yamamoto, 2017b: Spatial contrast of geographically induced rainfall observed by TRMM PR. *J. Climate*, **30**, 4165–4184.

Houze, R. A., Jr., 2004: Mesoscale convective systems. *Rev. Geophys.*, **42**, RG4003, doi:10.1029/2004RG000150.

Houze, R. A., Jr., K. L. Rasmussen, S. Medina, S. R. Brodzik, and U. Romatschke, 2011: Anomalous atmospheric events leading to the summer 2010 floods in Pakistan. *Bull. Amer. Meteor. Soc.*, **92**, 291–298.

Houze, R. A., Jr., K. L. Rasmussen, M. D. Zuluaga, and S. R. Brodzik, 2015: The variable nature of convection in the tropics and subtropics: A legacy of 16 years of the Tropical Rainfall Measuring Mission satellite. *Rev. Geophys.*, **53**, 994–1021.

Huffman, G. J., R. F. Adler, D. T. Bolvin, G. Gu, E. J. Nelkin, K. P. Bowman, Y. Hong, E. F. Stocker, and D. B. Wolff, 2007: The TRMM Multisatellite Precipitation Analysis (TMPA): Quasi-global, multiyear, combined-sensor precipitation estimates at fine scales. *J. Hydrometeor.*, **8**, 38–55.

Jain, D., A. Chakraborty, and R. S. Nanjundaiah, 2018: A mechanism for the southward propagation of mesoscale convective systems over the Bay of Bengal. *J. Geophys. Res.: Atmos.*, **123**, 3893–3913.

Jou, B. J.-D., W.-C. Lee, and R. H. Johnson, 2011: An overview of SoWMEX/TiMREX. *The Global Monsoon System*. Chang, C.-P., Y. Ding, N.-C. Lau, R. H. Johnson, B. Wang, and T. Yasunari (eds.), World Scientific, 303–318.

Kilpatrick, T., S.-P. Xie, and T. Nasuno, 2017: Diurnal convection-wind coupling in the Bay of Bengal. *J. Geophys. Res.: Atmos.*, **122**, 9705–9720.

Kirstetter, P.-E., Y. Hong, J. J. Gourley, M. Schwaller, W. A. Petersen, and J. Zhang, 2012: Comparison of TRMM 2A25 products, version 6 and version 7, with NOAA/NSSL ground radar–based national mosaic QPE. *J. Hydrometeor.*, **14**, 661–669.

Lim, S. Y., C. Marzin, P. Xavier, C.-P. Chang, and B. Timbal, 2017: Impacts of boreal winter monsoon cold surges and the interaction with MJO on Southeast Asia rainfall. *J. Climate*, **30**, 4267–4281.

Liu, C., 2011: Rainfall contributions from precipitation systems with different sizes, convective intensities, and

durations over the tropics and subtropics. *J. Hydrometeor.*, **12**, 394–412.

Liu, C., and M. W. Moncrieff, 1998: A numerical study of the diurnal cycle of tropical oceanic convection. *J. Atmos. Sci.*, **55**, 2329–2344.

Liu, C., M. W. Moncrieff, and J. D. Tuttle, 2008: A note on propagating rainfall episodes over the Bay of Bengal. *Quart. J. Roy. Meteor. Soc.*, **134**, 787–792.

Liu, C., E. J. Zipser, D. J. Cecil, S. W. Nesbitt, and S. Sherwood, 2008a: A cloud and precipitation feature database from nine years of TRMM observations. *J. Appl. Meteor. Climatol.*, **47**, 2712–2728.

Liu, C., E. J. Zipser, G. G. Mace, and S. Benson, 2008b: Implications of the differences between daytime and nighttime CloudSat observations over the tropics. *J. Geophys. Res.*, **113**, D00A04, doi:10.1029/2008JD009783.

Liu, Z., D. Ostrenga, W. Teng, and S. Kempler, 2012: Tropical Rainfall Measuring Mission (TRMM) precipitation data and services for research and applications. *Bull. Amer. Meteor. Soc.*, **93**, 1317–1325.

Rasmussen, K. L., and R. A. Houze, 2012: A flash-flooding storm at the steep edge of high terrain: Disaster in the Himalayas. *Bull. Amer. Meteor. Soc.*, **93**, 1713–1724.

Rasmussen, K. L., S. L. Choi, M. D. Zuluaga, and R. A. Houze, Jr., 2013: TRMM precipitation bias in extreme storms in South America. *Geophys. Res. Lett.*, **40**, 3457–3461.

Rasmussen, K. L., A. J. Hill, V. E. Toma, M. D. Zuluaga, P. J. Webster, and R. A. Houze, Jr., 2015: Multiscale analysis of three consecutive years of anomalous flooding in Pakistan. *Quart. J. Roy. Meteor. Soc.*, **141**, 1259–1276.

Romatschke, U., S. Medina, and R. A. Houze, Jr., 2010: Regional, seasonal, and diurnal variations of extreme convection in the South Asian region. *J. Climate*, **23**, 419–439.

Sato, T., 2013: Mechanism of orographic precipitation around the Meghalaya plateau associated with intraseasonal oscillation and the diurnal cycle. *Mon. Wea. Rev.*, **141**, 2451–2466.

Shige, S., Y. Nakano, and M. K. Yamamoto, 2017: Role of orography, diurnal cycle, and intraseasonal oscillation in summer monsoon rainfall over the Western Ghats and Myanmar coast. *J. Climate*, **30**, 9365–9381.

Shimpo, A., K. Takemura, S. Wakamatsu, H. Togawa, Y. Mochizuki, M. Takekawa, S. Tanaka, K. Yamashita, S. Maeda, R. Kurora, H. Murai, N. Kitabatake, H. Tsuguti, H. Mukougawa, T. Iwasaki, R. Kawamura, M. Kimoto, I. Takayabu, Y. N. Takayabu, Y. Tanimoto, T. Hirooka, Y. Masumoto, M. Watanabe, K. Tsuboki, and H. Nakamura, 2019: Primary factors behind the Heavy Rain Event of July 2018 and the subsequent heat wave in Japan. *SOLA*, **15A**, 13–18.

Su, S.-H., H.-C. Kuo, L.-H. Hsu, and Y.-T. Yang, 2012: Temporal and spatial characteristics of typhoon extreme rainfall in Taiwan. *J. Meteor. Soc. Japan*, **90**, 721–736.

Sui, C.-H., K.-M. Lau, Y. N. Takayabu, and D. A. Short, 1997: Diurnal variations in tropical oceanic cumulus convection during TOGA COARE. *J. Atmos. Sci.*, **54**, 639–655.

Takahashi, H. G., H. Fujinami, T. Yasunari, and J. Matsumoto, 2010: Diurnal rainfall pattern observed by Tropical Rainfall Measuring Mission Precipitation Radar (TRMM-PR) around the Indochina peninsula. *J. Geophys. Res.*, **115**, D07109, doi:10.1029/2009JD012155.

Tsai, W.-M., and C.-M. Wu, 2017: The environment of aggregated deep convection. *J. Adv. Model. Earth Syst.*, **9**, 2061–2078.

Weisz, E., J. Li, W. P. Menzel, A. K. Heidinger, B. H. Kahn, and C.-Y. Liu, 2007: Comparison of AIRS, MODIS, CloudSat and CALIPSO cloud top height retrievals. *Geophys. Res. Lett.*, **34**, L17811, doi:10.1029/2007GL030676.

Wicaksono, G. B., and R. Hidayat, 2016: Extreme rainfall in Katulampa associated with the atmospheric circulation. *Procedia Environ. Sci.*, **33**, 155–166.

Xu, W., E. J. Zipser, Y.-L. Chen, C. Liu, Y.-C. Liou, W.-C. Lee, and B. J.-D. Jou, 2012: An orography-associated extreme rainfall event during TiMREX: Initiation, storm evolution, and maintenance. *Mon. Wea. Rev.*, **140**, 2555–2574.

Yokoyama, C., H. Tsuji, and Y. N. Takayabu, 2020: The effects of an upper-tropospheric trough on the heavy rainfall event in July 2018 over Japan. *J. Meteor. Soc. Japan*, **98**, 235–255.

Zhou, L., and Y. Wang, 2006: Tropical rainfall measuring mission observation and regional model study of precipitation diurnal cycle in the New Guinean region. *J. Geophys. Res.*, **111**, D17104, doi:10.1029/2006JD007243.

Zipser, E. J., D. J. Cecil, C. Liu, S. W. Nesbitt, and D. P. Yorty, 2006: Where are the most intense thunderstorms on earth? *Bull. Amer. Meteor. Soc.*, **87**, 1057–1072.

Zuidema, P., 2003: Convective clouds over the Bay of Bengal. *Mon. Wea. Rev.*, **131**, 780–798.